Collisional–radiative model of neon discharge: determination of E/N in the positive column of low pressure discharge

2007 J. Phys. D: Appl. Phys. 40 1037

(http://iopscience.iop.org/0022-3727/40/4/018)

INSTITUTE OF PHYSICS PUBLISHING JOURNAL OF PHYSICS D: APPLIED PHYSICS

J. Phys. D: Appl. Phys. **40** (2007) 1037–1046 doi:10.1088/0022-3727/40/4/018

Collisional–radiative model of neon discharge: determination of E/N in the positive column of low pressure discharge

Z Navrátil[1,2], D Trunec[1], V Hrachová[3] and A Kaňka[3]

[1] Faculty of Science, Department of Physical Electronics, Masaryk University, Kotlářská 2, 611 37 Brno, Czech Republic
[2] Faculty of Science, Department of General Physics, Masaryk University, Kotlářská 2, 611 37 Brno, Czech Republic
[3] Faculty of Mathematics and Physics, Department of Electronics and Vacuum Physics, Charles University in Prague, V Holešovičkách 2, 182 00 Prague, Czech Republic

E-mail: zdenek@physics.muni.cz

Received 10 October 2006, in final form 4 December 2006
Published 2 February 2007
Online at stacks.iop.org/JPhysD/40/1037

Abstract

A method for the determination of the reduced electric field strength (E/N) in a neon discharge from the optical emission spectra was developed. This method is based on a collisional–radiative model, which was used to calculate the emission spectra of the neon plasma. In the model, populations of 30 excited levels of the neon atom were studied. Various elementary collision processes were taken into account: electron impact excitation, de-excitation and ionization of neon atoms, emission and absorption of radiation, metastable–metastable collisions, metastable and radiative dimer production, Penning ionization, etc. To determine the rates of electron collisions, the Boltzmann kinetic equation for the electron distribution function (EDF) was solved for given E/N, and thus the dependence of the emission spectra on E/N could be determined. The EDF was expanded in terms of Legendre polynomials and the first two terms of this approximation were taken into account. The theoretical emission spectra were fitted by the non-linear least-squares method to the measured spectra with respect to the unknown parameter E/N.

The method was applied to the study of low pressure dc glow discharge in neon. In such a discharge the calculated reduced electric field strength could be compared with the independent results of simultaneously performed electric probe measurements of E/N. Generally, close agreement of the calculated values with the experimental data was achieved.

(Some figures in this article are in colour only in the electronic version)

1. Introduction

Collisional–radiative models represent an important method in plasma studies. Basically, using the elementary data (cross sections, rate constants and transition probabilities) they enable the determination of population distributions of atoms, molecules and ions over their excited states. The knowledge of population distribution and its dependence on plasma parameters can be used in various ways: in diagnostics to determine the parameters of the studied plasma, in simulations, for example, to determine the discharge emission of radiation over a large range of conditions, or in atomic physics to study the elementary processes, which are responsible for population and depopulation of atomic excited levels.

A large number of collisional–radiative models has been reported in the literature, so only some of them are mentioned here. A very useful overview of collisional–radiative models was presented in [1]. A collisional–radiative

model with the Boltzmann solver was used to determine the stepwise excitation cross sections of rare-gas atoms in [2]. An extensive collisional–radiative model for argon [3, 4] enabled the investigation of population mechanisms of excited levels in various argon discharges. The method of electron temperature measurement, based on a collisional–radiative model, was reported in [5]. Collisional–radiative modelling was also employed in optical diagnostic methods used for the investigation of collisional processes governing the populations of the lowest 15 levels of the neon atom [6]. A collisional–radiative model for the study of positive columns of low pressure discharge in neon, argon and xenon was reported in [7].

In this paper the collisional–radiative model is used to develop the diagnostic method of reduced electric field strength (E/N) determination in neon discharges. Based on optical emission spectroscopy and on comparison of the measured spectra with the spectra calculated by the model, this method is entirely non-invasive and can be used under conditions when the electric probe measurement is not applicable or strongly disrupts the plasma (e.g. in atmospheric pressure discharges). However, in order to check the possibilities and limitations of this method, the model was applied to the study of the positive column of low pressure dc glow discharge in neon first. In such a discharge an independent electric probe measurement is possible and the results of both methods can be compared.

The paper is organized as follows: the collisional–radiative model and the method of determination of the reduced electric field strength is described in section 2. Details of the experimental apparatus, used for spectroscopy and probe measurements, are given in section 3. The results of both experimental and theoretical studies are presented, compared and discussed in section 4. Conclusions are presented in section 5.

2. Principles

The principal scheme of the method is shown in figure 1. An electron distribution function (EDF) was determined for a given E/N by a solution of the Boltzmann kinetic equation. After that, rate coefficients of electron collisions, which are responsible for the population (and the depopulation) of excited levels, could be determined. These rate coefficients, together with the rate coefficients and transition probabilities of other incorporated processes (e.g. electron impact ionization of neon atoms, emission and absorption of radiation, metastable–metastable collisions, three-body ion conversion, metastable and radiative dimer production and Penning ionization), served to build up the rate equations for concentrations of excited states of neon atoms. The steady state values of excited state concentrations, commonly determined just by the solution of algebraic balance equations [1], were found by a more robust fourth-order Runge–Kutta method with an adaptive step size according to [8]. This method was used to calculate the time development of the excited state concentrations from the initial guess to the steady state values from the rate equations. The calculated steady state populations allowed us to determine the optical emission spectrum for a given E/N, which was fitted by the least-squares method to the measured spectrum in order to determine the E/N in the discharge.

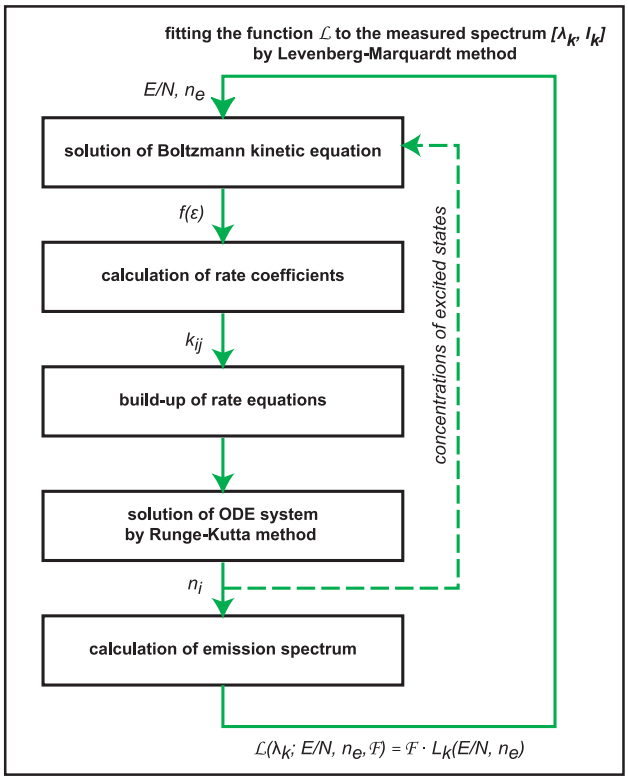

Figure 1. Principal scheme of method used for the determination of reduced electric field strength E/N. For explanation see the text.

In the following subsections more detailed descriptions of the above-mentioned procedures are given.

2.1. Electron distribution function

In order to obtain a distribution function of electrons in the positive column of a dc glow discharge a stationary Boltzmann kinetic equation was solved. Provided that the electric field is spatially uniform, EDF f is rotationally symmetric in the velocity space around the direction of the electric field and it may be expanded in terms of Legendre polynomials of cos θ (θ is the angle between the velocity and the electric field strength):

$$f(v, \theta) = f_0(v) + f_1(v) \cos\theta + \ldots, \tag{1}$$

where v denotes the magnitude of velocity. A common Lorentz approximation takes into account only the first two terms of the expansion: an isotropic part f_0 of EDF and an anisotropic perturbation f_1. Since functions f_0 and f_1 depend only on the magnitude of velocity, they can be simply expressed as the functions of the electron energy ε (in eV). Thus, $f_0(\varepsilon)$ was determined numerically by solving the equation

$$\begin{aligned}
&\frac{1}{3}\left(\frac{E}{N}\right)^2 \frac{\mathrm{d}}{\mathrm{d}\varepsilon}\left(\frac{\varepsilon}{\sigma_\mathrm{m}(\varepsilon)}\frac{\mathrm{d}f_0(\varepsilon)}{\mathrm{d}\varepsilon}\right) \\
&\quad + \frac{2m_\mathrm{e}}{M}\frac{\mathrm{d}}{\mathrm{d}\varepsilon}\left(\varepsilon^2\sigma_\mathrm{m}(\varepsilon)\left(f_0(\varepsilon) + \frac{k_\mathrm{b}T_\mathrm{n}}{e}\frac{\mathrm{d}f_0(\varepsilon)}{\mathrm{d}\varepsilon}\right)\right) \\
&\quad + \sum_{a,i,j}\frac{n_a}{N}[(\varepsilon+\varepsilon_{ij})f_0(\varepsilon+\varepsilon_{ij})\sigma_{ij}(\varepsilon+\varepsilon_{ij}) \\
&\quad - \varepsilon f_0(\varepsilon)\sigma_{ij}(\varepsilon)] = 0,
\end{aligned} \tag{2}$$

where E denotes the electric field, N is the concentration of neutral gas atoms, M their mass, m_e the electron mass, σ_m the momentum transfer cross section, k_b the Boltzmann constant, e the elementary charge and T_n the temperature of neutral atoms. n_a is the concentration of particles a, colliding inelastically with electrons (ground-state and excited atoms). ε_{ij} is the energy difference between the initial (ith) and final (jth) states of the colliding particles, which is positive in the case of excitation or ionization collisions and negative in the case of de-excitation collisions (superelastic electron collisions). σ_{ij} is the cross section of the collisions.

The binary excitation and ionization electron collisions with the ground-state neon atoms and excitation, ionization and de-excitation collisions with the neon atoms in $2p^5 3s$ states were taken into account as inelastic electron collisions. Details of the cross-section data being used are given in section 2.3. Assuming the following normalization of the EDF

$$\int_0^\infty f_0(\varepsilon)\varepsilon^{1/2}\,\mathrm{d}\varepsilon = 1, \tag{3}$$

the rate coefficient k of electron collisions with the cross-section σ can be calculated as

$$k = \sqrt{\frac{2e}{m_e}}\int_0^\infty \sigma(\varepsilon) f_0(\varepsilon)\varepsilon\,\mathrm{d}\varepsilon. \tag{4}$$

In such a way the rate coefficients of excitation and ionization electron collisions can be determined. The rate coefficients of electron de-excitation collisions were determined on the basis of a detailed balance between the two levels. Assuming σ for excitation cross section, the rate coefficient of inverse de-excitation collisions is

$$k = \sqrt{\frac{2e}{m_e}}\frac{g_j}{g_i}\int_{\varepsilon_{ij}}^\infty \sigma(\varepsilon) f_0(\varepsilon-\varepsilon_{ij})\varepsilon\,\mathrm{d}\varepsilon, \tag{5}$$

where ε_{ij} is the electron energy gain in de-excitation collisions and g_i, g_j are the statistical weights of upper and lower states of the colliding atom.

2.2. Excited levels

The 30 lowest excited states of the neon atom were incorporated in the collisional–radiative model. These states are listed, together with their notation, statistical weights and excitation energies, in table 1; their structure is schematically shown in figure 2. The ground state of the neon atom is a closed shell, $1s^2\,2s^2\,2p^6$. The four lowest excited states arise from the $2p^5 3s$ configuration. The states $1s_2$ and $1s_4$ (labelled in Paschen notation) are resonance levels with short radiative lifetimes. The spectral lines originating from transitions from these levels lie in the deep UV region (73.6 and 74.3 nm) and thus they are not measurable with the common UV-VIS optical spectrometers. The other states $1s_3$ and $1s_5$ are metastable with radiative lifetimes in the order of a second [9]. The next ten levels, $2p_1 - 2p_{10}$, are radiative states arising from the $2p^5 3p$ configuration. They are depopulated by intensive radiative transitions to $1s_2$–$1s_5$ states with wavelengths in the range 540–808 nm. These transitions are generally usable for optical diagnostics, since they occur even at low electric field strengths. Higher states $2s_i$, $3s_i$ and $3d_i$ arising from configurations $2p^5 4s$ and $2p^5 3d$ are upper states only for the transitions directed to the ground state and to the states of the $2p^5 3p$ configuration due to the selection rules. Under the conditions being considered the lines corresponding to these transitions are too weak or in the deep UV region to be used for diagnostics. Similar results were also obtained for higher excited states. Thus, only transitions $2p_i \to 1s_j$ were studied in the experiment. Inclusion of the states of $2p^5 4s$ and $2p^5 3d$ configurations in the model thus serves only to take into account the cascade contributions to $2p_i$ state excitations.

Table 1. The ground state and excited states of the neon atom, which were incorporated in the model. The individual columns show the effective level number i, describing the level in this paper, the $nlpqr$ number, the Racah and Paschen notation, statistical weight g_i and excitation energy $\mathcal{E}_i^{\mathrm{excit}}$ (according to [10]). The levels 26 and 27 are effective, both consisting of two real levels due to their unresolved excitation cross-section data.

Level i	Notation			g_i	$\mathcal{E}_i^{\mathrm{excit}}$ (eV)
	$nlpqr$	Racah	Paschen		
1	21000	$2p^6$	$1p_0$	1	0.00000
2	30332	$3s\,[3/2]_2^o$	$1s_5$	5	16.61907
3	30331	$3s\,[3/2]_1^o$	$1s_4$	3	16.67083
4	30110	$3s'[1/2]_0^o$	$1s_3$	1	16.71538
5	30111	$3s'[1/2]_1^o$	$1s_2$	3	16.84805
6	31311	$3p\,[1/2]_1$	$2p_{10}$	3	18.38162
7	31353	$3p\,[5/2]_3$	$2p_9$	7	18.55511
8	31352	$3p\,[5/2]_2$	$2p_8$	5	18.57584
9	31331	$3p\,[3/2]_1$	$2p_7$	3	18.61271
10	31332	$3p\,[3/2]_2$	$2p_6$	5	18.63679
11	31131	$3p'[3/2]_1$	$2p_5$	3	18.69336
12	31132	$3p'[3/2]_2$	$2p_4$	5	18.70407
13	31310	$3p\,[1/2]_0$	$2p_3$	1	18.71138
14	31111	$3p'[1/2]_1$	$2p_2$	3	18.72638
15	31110	$3p'[1/2]_0$	$2p_1$	1	18.96596
16	40332	$4s\,[3/2]_2^o$	$2s_5$	5	19.66403
17	40331	$4s\,[3/2]_1^o$	$2s_4$	3	19.68820
18	40110	$4s'[1/2]_0^o$	$2s_3$	1	19.76060
19	40111	$4s'[1/2]_1^o$	$2s_2$	3	19.77977
20	32310	$3d\,[1/2]_0^o$	$3d_6$	1	20.02464
21	32311	$3d\,[1/2]_1^o$	$3d_5$	5	20.02645
22	32374	$3d\,[7/2]_4^o$	$3d'_4$	9	20.03465
23	32373	$3d\,[7/2]_3^o$	$3d_4$	7	20.03487
24	32332	$3d\,[3/2]_2^o$	$3d_3$	5	20.03675
25	32331	$3d\,[3/2]_1^o$	$3d_2$	3	20.04039
26	32352	$3d\,[5/2]_2^o$	$3d''_1$	5	20.04821
	32353	$3d\,[5/2]_3^o$	$3d'_1$	7	20.04843
27	32152	$3d'[5/2]_2^o$	$3s'''_1$	5	20.13611
	32153	$3d'[5/2]_3^o$	$3s'''_1$	7	20.13630
28	32132	$3d'[3/2]_2^o$	$3s''_1$	5	20.13751
29	32131	$3d'[3/2]_1^o$	$3s'_1$	3	20.13946

2.3. Considered elementary processes

Various collisional, radiative and also diffusion processes, governing the populations of the considered 30 excited neon states, were taken into account[4].

(i) Electron impact excitation out of the ground state and the $2p^5 3s$ states:

$$\mathrm{Ne}(i) + \mathrm{e}^- \xrightarrow{k_{ij}} \mathrm{Ne}(j) + \mathrm{e}^-,$$
$$i = 1,\ldots 5, \qquad j = 2,\ldots 29, \qquad i < j. \tag{6}$$

[4] The neon excited states are distinguished in the following list by a level number i, which is written in parentheses after the element symbol (see table 1).

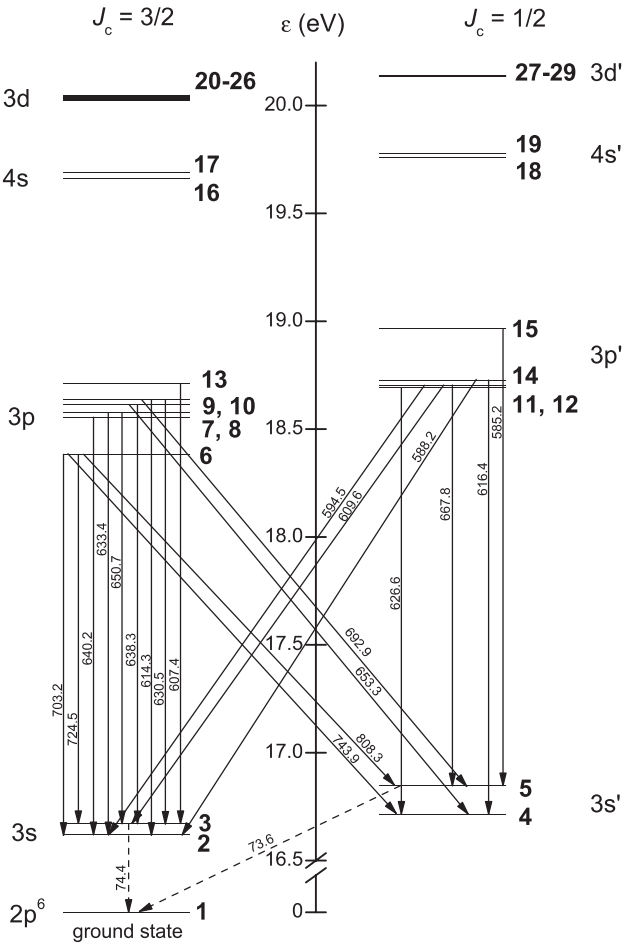

Figure 2. The scheme of excited levels of the neon atom showing the levels incorporated in the model and the main radiative transitions from 3s and 3p states. The number in bold face denotes the effective level number.

(ii) Electron impact de-excitation to the ground state and the $2p^5 3s$ states:

$$\mathrm{Ne}(i) + \mathrm{e}^- \xrightarrow{k_{ij}} \mathrm{Ne}(j) + \mathrm{e}^-, \quad i = 2, \ldots 29, \quad j = 1, \ldots 5, \quad i > j. \tag{7}$$

(iii) Spontaneous emission of radiation:

$$\mathrm{Ne}(i) \xrightarrow{A_{ij}} \mathrm{Ne}(j) + h\nu, \quad i = 2, \ldots 29, \quad i > j. \tag{8}$$

Symbol A_{ij} denotes the Einstein coefficient of spontaneous emission.

(iv) Absorption of radiation:

$$\mathrm{Ne}(i) + h\nu \xrightarrow{(1-\Lambda_{ji})A_{ji}} \mathrm{Ne}(j), \quad i = 1, \ldots 28, \quad i < j. \tag{9}$$

Symbol Λ_{ji} denotes the escape factor (see section 2.4).

(v) Electron impact ionization of the ground-state and metastable atoms:

$$\mathrm{Ne}(1) + \mathrm{e}^- \xrightarrow{k_{\mathrm{ion}}} \mathrm{Ne}^+ + \mathrm{e}^- + \mathrm{e}^-, \tag{10}$$

$$\mathrm{Ne}(2,4) + \mathrm{e}^- \xrightarrow{k_{\mathrm{ionmet}}} \mathrm{Ne}^+ + \mathrm{e}^- + \mathrm{e}^-. \tag{11}$$

(vi) Chemoionization:

$$\mathrm{Ne}(2,4) + \mathrm{Ne}(2,4) \xrightarrow{k_{\mathrm{met}}} \mathrm{Ne}(1) + \mathrm{Ne}^+ + \mathrm{e}^-. \tag{12}$$

(vii) Associative ionization:

$$\mathrm{Ne}(2,4) + \mathrm{Ne}(2,4) \xrightarrow{k_{\mathrm{met}}} \mathrm{Ne}_2^+ + \mathrm{e}^-. \tag{13}$$

(viii) Collision-induced emission:

$$\mathrm{Ne}(2,4) + \mathrm{Ne}(1) \xrightarrow{k_{2\mathrm{b}}} 2\mathrm{Ne}(1) + h\nu. \tag{14}$$

(ix) Three-body production of dimers:

$$\mathrm{Ne}(2,4) + \mathrm{Ne}(1) + \mathrm{Ne}(1) \xrightarrow{k_{3\mathrm{b_m}}} \mathrm{Ne}_2^* + \mathrm{Ne}(1), \tag{15}$$

$$\mathrm{Ne}(3) + \mathrm{Ne}(1) + \mathrm{Ne}(1) \xrightarrow{k_{3\mathrm{b_3}}} \mathrm{Ne}_2^m + \mathrm{Ne}(1), \tag{16}$$

$$\mathrm{Ne}(5) + \mathrm{Ne}(1) + \mathrm{Ne}(1) \xrightarrow{k_{3\mathrm{b_5}}} \mathrm{Ne}_2^m + \mathrm{Ne}(1). \tag{17}$$

(x) Penning ionization of impurities (concentrations according to the gas supplier specification):

$$\mathrm{Ne}(2\text{–}5) + \mathrm{H}_2 \xrightarrow{k_{\mathrm{H}_2^+}} \mathrm{H}_2{}^+ + \mathrm{Ne}(1) + \mathrm{e}^-, \tag{18}$$

$$\mathrm{Ne}(2\text{–}5) + \mathrm{H}_2 \xrightarrow{k_{\mathrm{NeH}^+}} \mathrm{NeH}^+ + \mathrm{H} + \mathrm{e}^-, \tag{19}$$

$$\mathrm{Ne}(2\text{–}5) + \mathrm{N}_2 \xrightarrow{k_{\mathrm{N}_2^+}} \mathrm{N}_2{}^+ + \mathrm{Ne}(1) + \mathrm{e}^-, \tag{20}$$

$$\mathrm{Ne}(2\text{–}5) + \mathrm{N}_2 \xrightarrow{k_{\mathrm{NeN}_2^+}} \mathrm{NeN}_2{}^+ + \mathrm{e}^-, \tag{21}$$

$$\mathrm{Ne}(2\text{–}5) + \mathrm{O}_2 \xrightarrow{k_{\mathrm{O}_2^+}} \mathrm{O}_2{}^+ + \mathrm{Ne}(1) + \mathrm{e}^-. \tag{22}$$

These processes were incorporated for generality. However, we assume a negligible influence on the calculated spectra.

(xi) Diffusion of metastable-state atoms to the wall.

The rate coefficients for excitation of neon atoms by electron impact k_{ij} ($i < j$) were calculated according to (4). The cross-section data in [11] were adapted for the direct excitation of the ground-state neon atoms into both metastable states $1s_3$, $1s_5$ of the $2p^5 3s$ configuration. The data for direct excitation into radiative states $1s_2$, $1s_4$ of the $2p^5 3s$ configuration were taken from [12, 13]. To calculate the direct excitation into the states of $2p^5 3p$, $2p^5 4s$ and $2p^5 3d$ configurations the data published in [14] and [15], respectively, were used.

The experimental values of cross sections in [16] were used for the excitation out of states of the $2p^5 3s$ configuration. However, in this work only the cross sections (given in absolute values) for excitation out of the state $1s_5$ (effective number 2) into states $2p_9$ (7), $2p_8$ (8), $2p_6$ (10) and $2p_4$ (12) were published. The cross sections for other states were presented, e.g. in [2, 17, 18][5], but the reported values differ considerably for some transitions from the recent data published in [16].

[5] The average cross section for excitation among the states $2p^5$ 3s–$2p^5$ 3p was published in [18].

Table 2. Rate coefficients of the processes considered in the model. The number in parentheses, if appropriate, denotes the level, for which the value is valid.

Denomination	Value	References
k_{ij}	calculated	[11–14,16]
k_{ion}	calculated; (1)	[11]
k_{ionmet}	calculated; (2, 4)	[22]
k_{met}	6.40×10^{-16} m^3 s^{-1}; (2, 4)	[24]
$k_{2\mathrm{b}}$	1.55×10^{-21} m^3 s^{-1}; (2, 4)	[24]
$k_{3\mathrm{b_m}}$	5.00×10^{-46} m^6 s^{-1}; (2, 4)	[25]
$k_{3\mathrm{b_3}}$	7.04×10^{-45} m^6 s^{-1}; (3)	[26]
$k_{3\mathrm{b_5}}$	6.45×10^{-46} m^6 s^{-1}; (5)	[26]
$k_{\mathrm{H_2^+}}$	1.79×10^{-17} m^3 s^{-1}; (2–5)	[27]
$k_{\mathrm{NeH^+}}$	0.51×10^{-17} m^3 s^{-1}; (2–5)	[27]
$k_{\mathrm{N_2^+}}$	7.52×10^{-17} m^3 s^{-1}; (2–5)	[27]
$k_{\mathrm{NeN_2^+}}$	0.48×10^{-17} m^3 s^{-1}; (2–5)	[27]
$k_{\mathrm{O_2^+}}$	2.50×10^{-16} m^3 s^{-1}; (2–5)	[27]
D_2N	5.1×10^{20} m^{-1} s^{-1}; (2, 300 K)	[25]
D_4N	5.8×10^{20} m^{-1} s^{-1}; (4, 300 K)	[25]

According to [19], the cross sections scale with the oscillator strengths also at low electron energies, where the Born approximation of excitation cross section is not valid. Thus, the excitation function for the $1s_5$–$2p_9$ transition published in [16] was scaled with the oscillator strength ratio to obtain a consistent set of excitation cross sections for optically allowed transitions among the states $2p^53s$–$2p^53p$. Two different sets of cross sections for the $2p^53s$–$2p^53p$ excitations were tested: the set consisting of the four cross sections from [16] (Set 1) and the set expanded with the cross sections for other transitions determined by scaling the cross section for the $1s_5$–$2p_9$ excitation (Set 2). The cross sections for optically forbidden transitions, which could not be determined in this way, were assumed to be zero.

The rate coefficients for de-excitation of neon atoms by electron impact k_{ij} ($i > j$) were calculated according to (5) from the same excitation cross-section data. The rate coefficients for ionization of neon atoms by electron impact k_{ion} (ground-state atoms) and k_{ionmet} (metastables) were determined again from (4). The cross section for direct ionization by electron impact was taken from [11], where early measurements in [20, 21] were combined. Ionization of neon metastables was characterized by cross-section data published in [22]. The same cross-section values for both metastable states were assumed as in this reference.

The Einstein coefficients for spontaneous emission A_{ij} were taken primarily from [10]. The transition probability data, which were not included in this database, were taken from [23]. The transition probabilities of effective levels 26 and 27 were determined as

$$A_{\{i\}j} = \frac{\sum_i g_i A_{ij}}{\sum_i g_i}, \qquad i \in \{i\}, \tag{23}$$

in which A_{ij} is the Einstein coefficient, g_i the statistical weight and i indexes the levels grouped into an effective level $\{i\}$.

The rate coefficients for collisions, in which heavy particles (e.g. neon ground-state atoms and metastables) participate, are given with their references in table 2.

The rate equation for the concentration of excited state i of the neon atom has generally the form

$$\begin{aligned}\frac{\mathrm{d}n_i}{\mathrm{d}t} &= k_{1i}n_\mathrm{e}n_1 - k_{i1}n_\mathrm{e}n_i + \delta_{i\,3\mathrm{p}}\left(\sum_{j=2}^{5} k_{ji}n_\mathrm{e}n_j - \sum_{j=2}^{5} k_{ij}n_\mathrm{e}n_i\right) \\ &+ \delta_{i\,3\mathrm{s}}\Big(-\sum_{j=6}^{15} k_{ij}n_\mathrm{e}n_i + \sum_{j=6}^{15} k_{ji}n_\mathrm{e}n_j\Big) - \sum_{j=1}^{i-1}\Lambda_{ij}A_{ij}n_i \\ &+ \sum_{j=i+1}^{29}\Lambda_{ji}A_{ji}n_j = 0,\end{aligned} \tag{24}$$

where n_e and N denote the concentration of electrons and neutral atoms, respectively, $\delta_{i\,3\mathrm{p}}$ equals unity for $2p^53p$ levels (i = 6–15) and zero otherwise and $\delta_{i\,3\mathrm{s}}$ is defined similarly for $2p^53s$ levels (i = 2–5). The concentration of neutral atoms was determined from the thermodynamic equation of state. The rate equations for $2p^53s$ states and particularly for metastable states are more complicated, incorporating other, in some cases also non-linear, processes as mentioned above.

2.4. Radiation trapping

The radiation emitted by a single atom in the discharge can be absorbed and re-emitted by surrounding atoms many times before the radiation reaches the walls of the discharge chamber. This repeated absorption–re-emission process, known as radiation trapping, changes the apparent radiative lifetimes of states and transition probabilities. The radiation trapping is crucial in the case of resonance transitions, but it may be important also in the case of transitions with a metastable lower state. In collisional–radiative models the local effect of absorption of radiation is approximately described by so-called escape factors, which are calculated by solving the Holstein equation [28] for various discharge geometries and line shapes. In our calculations a technique described in [29] was adapted. In this work trapping factors g (inverse value to escape factor) were published for Doppler (g^D), Lorentz (g^L) and Voigt (g^V) line shapes and cylindrical and spherical geometries:

$$\begin{aligned}g^\mathrm{D}(k_0R) &= 1 + \frac{1}{m_j^\mathrm{D}}k_0R\sqrt{\ln\left(\frac{k_0R}{2} + \mathrm{e}\right)} \\ &- \frac{c_{0,j}^\mathrm{D}k_0R\ln(k_0R) + c_{1,j}^\mathrm{D}k_0R + c_{2,j}^\mathrm{D}(k_0R)^2}{1 + c_{3,j}^\mathrm{D}k_0R + c_{4,j}^\mathrm{D}(k_0R)^2},\end{aligned}$$

$$\begin{aligned}g^\mathrm{L}(k_0R) &= \frac{1}{m_j^\mathrm{L}}\sqrt{\pi k_0R + (m_j^\mathrm{L})^2} \\ &- \frac{c_{0,j}^\mathrm{L}k_0R\ln k_0R + c_{1,j}^\mathrm{L}k_0R + c_{2,j}^\mathrm{L}(k_0R)^2}{1 + c_{3,j}^\mathrm{L}k_0R + c_{4,j}^\mathrm{L}(k_0R)^2},\end{aligned}$$

$$\begin{aligned}g^\mathrm{m}(k_0R) &= 1 - \frac{1.5}{a+1}\left(\frac{k_0R}{k_0R + \alpha m_j^\mathrm{D}/m_j^\mathrm{L}}\right. \\ &\left. - \frac{k_0R}{k_0R + \beta m_j^\mathrm{D}/m_j^\mathrm{L}}\right),\end{aligned}$$

$$g^\mathrm{B}(k_0R) = 1 + \frac{1}{a}\sqrt{\pi\ln(k_0R + \mathrm{e})m_j^\mathrm{L}/m_j^\mathrm{D}},$$

Table 3. Constants for calculation of the trapping factor for discharge with cylindrical geometry (according to [29]).

i	0	1	2	3	4
$c^{\mathrm{D}}_{i,0}$	-4.447×10^{-3}	2.464×10^{-1}	-2.139×10^{-4}	1.650×10^{-2}	6.570×10^{-6}
$c^{\mathrm{L}}_{i,0}$	1.204×10^{-1}	8.738×10^{-1}	-3.321×10^{-3}	1.877	1.166×10^{-1}
m^{D}_0	8.889×10^{-1}				
m^{L}_0	1.1227				
α	4				
β	12				

$$g^{\mathrm{A}}(k_0R) = g^{\mathrm{L}}\left(\frac{k_0R}{a\sqrt{\pi}}\right) \Big/ g^{\mathrm{B}}(k_0R),$$

$$\frac{1}{g^{\mathrm{V}}(k_0R)} = \frac{\mathrm{e}^{-g^{\mathrm{A}^2}(k_0R)}}{g^{\mathrm{D}}(k_0R)}\left(1 - \frac{\sqrt{\pi}}{2}\frac{g^{\mathrm{A}}(k_0R)}{(1+k_0R/m^{\mathrm{D}}_j)^2}\right) + \frac{\mathrm{erf}[g^{\mathrm{A}}(k_0R)]}{g^{\mathrm{L}}[k_0R/(a\sqrt{\pi})]g^{\mathrm{m}}(k_0R)},$$

$$\Lambda^{\mathrm{V}}(k_0R) = \frac{1}{g^{\mathrm{V}}(k_0R)}. \tag{25}$$

In these equations k_0 is the absorption coefficient at the line centre, R the discharge radius and a the damping constant. $c^X_{i,j}$ and m^X_j are coefficients associated with the eigenfunction (or mode j) constituting the spatial dependence of the concentration of the excited state. The coefficients for the lowest mode ($j = 0$), as the only one, which was taken into account, and for cylindrical geometry, are listed in table 3. Constants α and β were determined by discharge geometry (see also table 3). In our calculations the Voigt profile was assumed and the damping constant a was calculated from the FWHMs (full widths at half of the maximum) of Doppler, Stark, natural and resonance broadening.

2.5. Comparison of the spectra

The measured spectrum and the spectra calculated for various values of E/N were compared in order to determine the E/N. Usually, for the determination of E/N the ratio of two spectral line intensities is used to avoid difficulties in absolute intensity measurements [30]. However, in order to achieve a reasonable sensitivity of this intensity ratio to the plasma parameters, a large difference in the excitation energies of the upper states of the two spectral lines used is needed. This requirement is in contrast to the availability of reliable cross-section data for highly excited levels. Moreover, under conditions studied in this paper (low reduced electric field strength) the lines originating from highly excited levels were not present in the measured spectrum and only the lines from $2\mathrm{p}_i$ states with a small energy spread of 0.6 eV could be studied. Thus, more lines ($n = 16$–20) were taken in the analysis. Assuming I_k and L_k for the measured and calculated intensity of line k, respectively, the spectra were compared on the basis of the least-squares sum

$$\mathcal{S} = \sum_{k=1}^{n}(\mathcal{F}\cdot L_k(E/N, n_{\mathrm{e}}) - I_k)^2, \tag{26}$$

where $\mathcal{F}$ is the scaling factor, adjusting the relative intensities of the spectra. If we define a function $\mathcal{L}$ as

$$\mathcal{L}(\lambda_k; E/N, n_{\mathrm{e}}, \mathcal{F}) = \mathcal{F}\cdot L_k(E/N, n_{\mathrm{e}}), \tag{27}$$

then the parameters E/N, n_{e} and $\mathcal{F}$ can be found by fitting the function $\mathcal{L}$ to the data

$$\{[\lambda_k, I_k],\ k = 1, \ldots, n\}. \tag{28}$$

The number of lines n ranged from 14 for the spectrum measured at a high electric field to 20 lines at a low electric field. The Marquardt–Levenberg algorithm of the least-squares method was used for fitting in order to minimize the time of calculation.

3. Experimental set-up

The measurements were carried out in a U-shaped Pyrex discharge tube with a total length of 590 mm. The central part of the discharge tube, 390 mm long, was equipped with Pyrex head-on-windows. The inner diameter of this part was 24 mm. The discharge tube was filled up to the working pressure of 1.1 Torr with spectrally pure neon produced by Moravské Chemické Závody Ostrava. The amount of impurities was below 10 ppm.

The U-shaped discharge tube enabled us to investigate the spectral line intensities of the discharge in the central part of the tube at the tube axis. The emitted light, averaged over the central part, was imaged by a positive lens onto a quartz fibre and analysed by a Jobin Yvon-Spex Triax 550 monochromator (focal length 550 mm) equipped with a plane grating (1200 grooves mm^{-1}) and a thermoelectrically cooled MTE CCD 1024×256-16 detector. The spectra were measured in the spectral range 300–850 nm for six values of discharge current.

The axial electric field strength was measured by a double probe method. The fixed probes were made from a platinum wire 100 μm in diameter and 3 mm in length. The active region of the probes was immersed into the positive column perpendicularly to the axis of the central part of the tube at the distance of 15 mm. The probe technique was also used to determine the electron concentration.

The optical system was calibrated with a Pencil style 6035 Hg(Ar) lamp produced by Oriel Instruments, operating in the dc mode at 18 mA. The irradiances of selected lines were taken from [31]. Due to the practically constant dependence of the quantum efficiency of our instrument on the wavelength (with error no more than 4%) in the measured range 560–750 nm, this calibration was extended to wavelengths higher than that provided by the lamp. Therefore, the relative intensities of the neon lines were determined with uncertainties of about 15% and even higher at wavelengths above 600 nm.

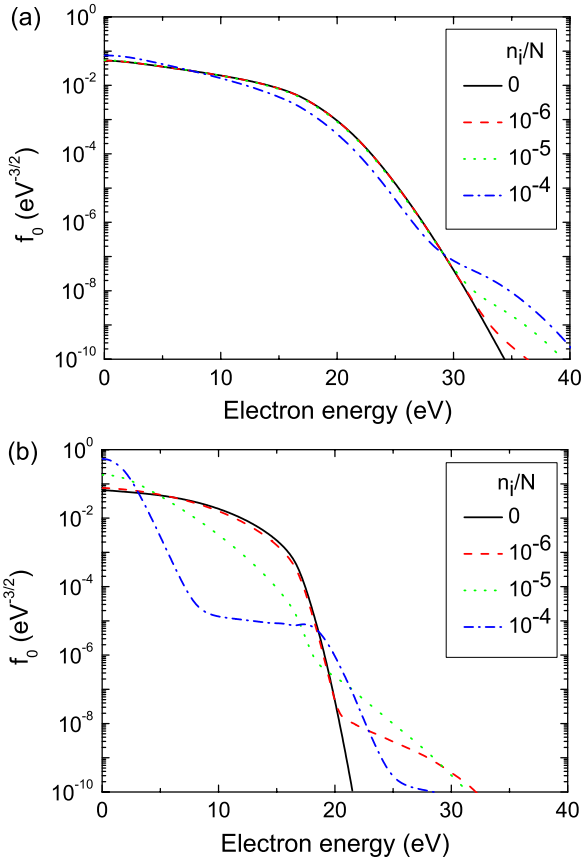

Figure 3. The isotropic part of EDF for reduced electric field strengths (*a*) $E/N = 12$ Td and (*b*) $E/N = 2$ Td and various relative concentrations n_i/N of individual $2p^5 3s$ states. The concentrations of all states of $2p^5 3s$ configuration are assumed to have the same value.

4. Results and discussion

The isotropic part of the EDF $f_0(\varepsilon)$ is shown for reduced electric field strengths 12 and 2 Td in figure 3. The effect of processes, in which neon atoms in the excited states of the $2p^5 3s$ configuration participate, on the EDF is documented by plots of the EDF for various concentrations of excited states. Since the de-excitation collisions accelerate the electrons, the increase in the concentration of the excited atoms is manifested in the increase in the number of energetic electrons in the tail of the EDF. In contrast, the excitation collisions of electrons with the atoms in $2p^5 3s$ states (of large collision cross sections) and ionization collisions with the metastables further increase the proportion of low energetic electrons in the EDF in comparison with the inclusion of excitation and ionization collisions out of the ground state only. As can be seen in the figure, the EDF seems to be much more sensitive to these processes at a lower value of reduced electric field strength. However, at a low electric field the relative concentrations of excited states, which were used in the calculations, are hardly attainable. The influence of electron–electron collisions on the EDF was found to be negligible under our experimental conditions (ionization degree $\sim 10^{-8}$, $n_e \sim 10^8$ cm^{-3}). These results are in agreement with the calculations presented for argon in [32] or for helium in [33].

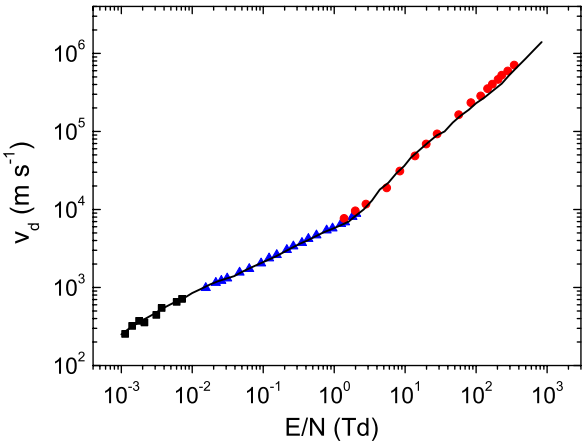

Figure 4. Calculated drift velocity v_d plotted as a function of reduced electric field strength E/N. The calculated curve (——) is compared with the experiments (■) [34], (▲) [35] and (●) [36].

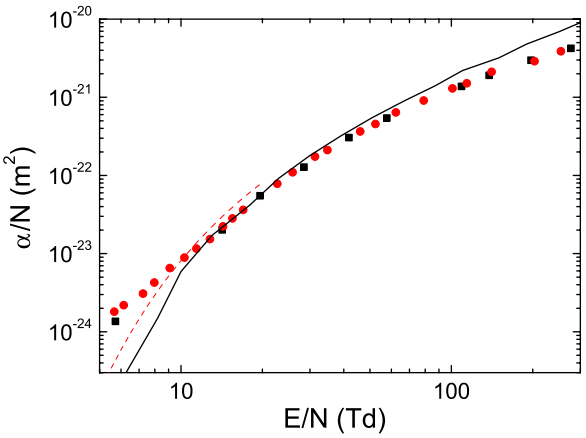

Figure 5. The calculated reduced Townsend ionization coefficient α/N as a function of the reduced electric field strength E/N for two different solutions of the Boltzmann kinetic equation: (——) without incorporation of excited states, (- - - -) with incorporation of excited states. The calculated curves are compared with the experiments (■) [37] and (●) [38].

The accuracy of the calculated EDF and of the used cross-section data was tested by a comparison of the transport parameters (calculated as the moments of EDF) with their experimental values. The dependence of drift velocity v_d on the reduced electric field strength is shown in figure 4. Close agreement of the calculated curve with the experimental data can be observed. However, as noted already in [11] and verified again by changing the cross-section set (not shown here), the drift velocity is less sensitive to excitation cross-section data.

A similar comparison of the reduced Townsend ionization coefficient, which was calculated as $\alpha/N = k_{ion}/v_d$, is shown in figure 5. The calculations are in agreement with the experimental data at middle reduced electric field strengths (10–100 Td). The discrepancy at higher values is particularly due to the limited electron energy range (up to 200 eV) of the used excitation cross sections, but such a discrepancy is unimportant for the diagnostics of the positive column plasma being studied in this paper. The discrepancy in the Townsend ionization coefficient at a low reduced electric field may be improved, aside from the explanation based on the

Table 4. Comparison of the calculated values of E/N determined from Fit 1 (cross-section set No. 1) and Fit 2 (cross-section set No. 2) with the results of probe measurement. The error estimates were calculated for the confidence level of 68.3 %.

Spectrum no.	Current (mA)	E/N (Td)		
		Measured	Fit 1	Fit 2
1	5	12.9 ± 1.2	12.4 ± 5.5	8.5 ± 4.3
2	10	8.1 ± 0.8	10.7 ± 3.9	5.6 ± 2.5
3	15	6.6 ± 0.7	8.6 ± 2.8	3.3 ± 3.1
4	20	6.2 ± 0.6	8.5 ± 2.7	4.7 ± 3.1
5	25	5.8 ± 0.6	8.7 ± 2.7	7.0 ± 3.2
6	30	5.3 ± 0.5	8.3 ± 2.5	6.9 ± 3.1

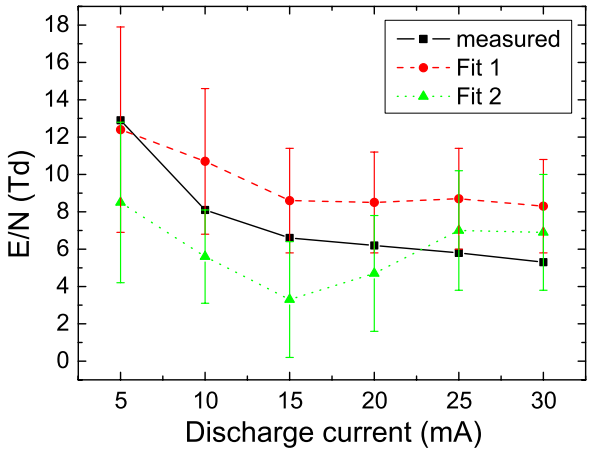

Figure 6. The reduced electric field strength versus the discharge current determined from Fit 1 and Fit 2 with different cross-section sets in comparison with the experimental data from the probe measurement.

overestimation of experimental data [11], by using the EDF, which was calculated with the excited states taken into account (see the dashed curve in figure 5). However, the collisional–radiative model is needed to determine the concentrations of excited atoms in such calculations.

The calculated values of the reduced electric field strength, determined from Fit 1 and Fit 2 with different cross-section sets No. 1 and No. 2 (described in section 2.3), are given together with the experimental data in table 4 and they are shown as functions of the discharge current in figure 6. The electron concentration was not found from the fits, since the ratios of the line intensities in the calculated spectra did not depend on the electron concentration significantly. The electron concentration acted only as another scaling factor and thus it was strongly correlated with the scaling factor $\mathcal{F}$. The measured values of the electric field strength generally lie within the confidence intervals determined from both fits, which were calculated for the probability level of 68.3%. Comparing the two fits, Fit 1 gives closer agreement with the experimental values, particularly at higher electric field (12 Td). At lower electric fields the agreement is worse, since the direct excitation becomes less intensive at a lower electric field and the model used thus becomes less sensitive. This was improved by the inclusion of the stepwise excitation through the states of the $2p^5 3s$ configuration in Fit 2. However, it was found that the total sum of the squares determined from Fit 2 was not reduced substantially and in some cases the sum was

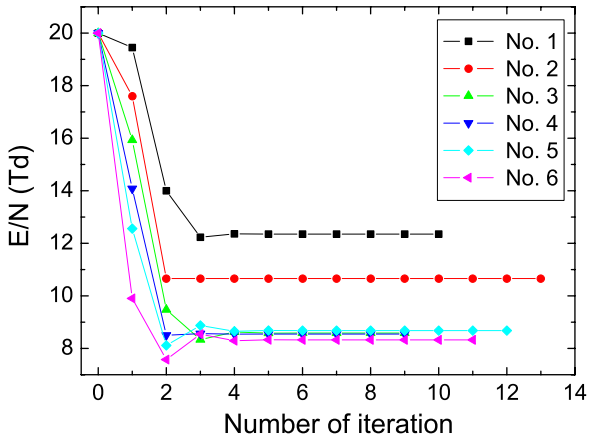

Figure 7. The example of the reduced electric field strength development during the iterations of the Marquardt–Levenberg algorithm on different spectra no. 1–6.

even higher than that of Fit 1. This result may be caused by various factors. The uncertainty of the collision cross sections of the $2p^5 3s$–$2p^5 3p$ excitation measured in [16] is about ±30% and the results of various authors differ even by a factor of 3. (The error of direct excitation cross sections is up to ±36% [14].) Furthermore, the omission of optically forbidden excitations may play some role, since these optically forbidden excitations may be due to the excitation functions with sharp maxima at low electron energies of significant importance at a low electric field. Finally, the uncertainty of the populations of $2p^5\,3s$ states is also included in the calculated spectra through the stepwise excitation. For example, the error of cross sections for excitation from the ground state to the $1s_4$ and $1s_2$ states was estimated to be ±20% [13] and the other uncertainty is caused, e.g., by errors in Einstein coefficients and approximate description of resonance radiation trapping.

The example of the development of electric field strength during the iterations of the Marquardt–Levenberg algorithm on different spectra is shown in figure 7. The initial value of E/N was set in all cases to 20 Td; the electron concentration was fixed at 10^8 cm^{-3} according to the experimental data. The iteration mostly tended to the resultant value after several (≈10) steps of the Marquardt–Levenberg algorithm. The examples of the fitted spectra are shown in figure 8. The solid line represents the measured spectrum, corrected in accordance with the spectrometer sensitivity, and the arrows denote the results of Fit 1. The fitted and measured intensities of spectral lines are generally in close agreement, with the exception of the lines in the red end of the spectrum. Since the lines 703.24, 724.52 and 743.89 nm start in the same upper state $2p_{10}$, their intensities should be approximately in the proportion of their Einstein coefficients. Since this is not observed in the measured spectrum, the discrepancy in the measured and calculated intensities is probably due to the overestimation of the measured intensities in the spectrum correction. The measured and the calculated intensity of the spectral line at 614.34 nm are obviously different as well. The upper level of the 614.34 nm transition was also populated by excitation out of the $1s_5$ level, so a large calculated intensity may arise, e.g., from an overestimation of the metastable atoms density (which can be expected due to the not fully included depopulation, e.g., by heavy-particle collisions).

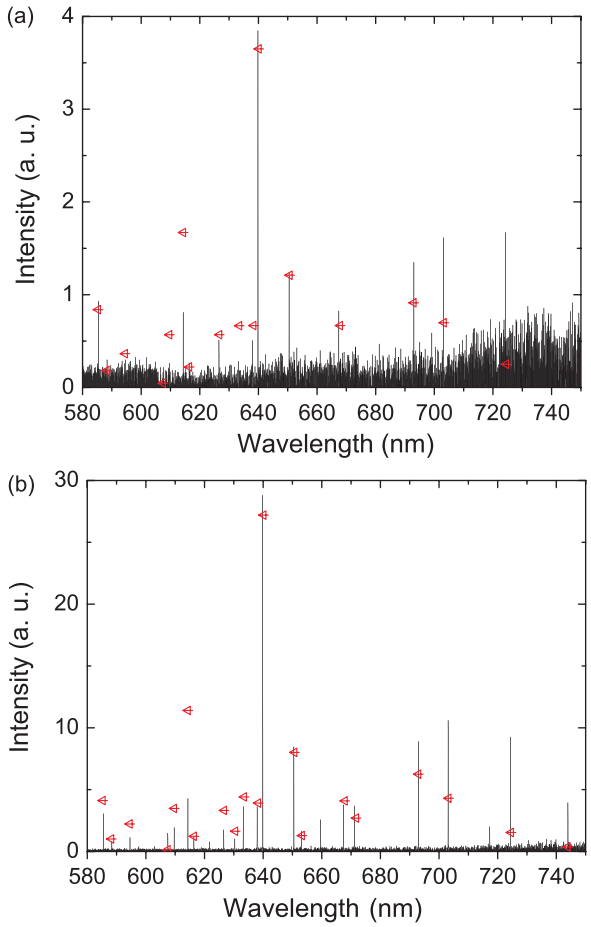

Figure 8. The examples of the measured spectra and the results of the fitting procedure shown by arrows (◁–). (*a*) Spectrum no. 1 and (*b*) spectrum no. 5.

5. Conclusion

The collisional–radiative model of the neon discharge was developed in order to determine the reduced electric field strength in the positive column of the low pressure dc glow discharge. The optical emission spectra, which were compared by the least-squares fitting method with the resultant spectra of the collisional–radiative model, were measured in the positive column of the discharge for six values of the discharge current. Furthermore, independent measurements of the electric field by electric probes were performed.

In the collisional–radiative model populations of 30 excited levels of the neon atom were studied. A number of elementary processes were taken into account: electron impact excitation, de-excitation and ionization of neon atoms, emission and absorption of radiation, metastable–metastable collisions, metastable and radiative dimer production, Penning ionization, etc. The electrons were characterized by the EDF in the two-term approximation, which was determined for a given E/N by the solution of the Boltzmann kinetic equation. The steady state values of populations of excited states were found by the solution of their rate equations by the Runge–Kutta method. The calculated spectra were fitted by the Marquardt–Levenberg least-squares algorithm to the measured spectrum in order to determine the E/N in the discharge.

The comparison of calculated and experimental results of E/N in the positive column of the low pressure dc glow discharge shows agreement of the measured and the calculated values. The calculated E/N values ranged from 3 to 12 Td depending on the discharge current. The model sensitivity to the E/N was found to be higher for higher E/N. The aim of the next work will be to apply this method to the study of discharges, at which the determination of the E/N by electric probe diagnostics is not possible (e.g. atmospheric pressure discharges).

Acknowledgments

The work was supported by the research project MSM0021622411 of the Ministry of Education of the Czech Republic and by grants nos 202/06/0776, 202/05/0777 and 202/06/1473 of the Czech Science Foundation. VH and AK acknowledge the support of the research project MSM 0021620834.

References

[1] van der Sijde B, van der Mullen J J A M and Schram D C 1984 Collisional radiative models in plasmas *Beitr. Plasmaphys.* **24** 447–73
[2] Behnke J F, Deutsch H and Scheibner H 1985 Investigation about stepwise excitation cross sections in rare gases *Contrib. Plasma Phys.* **25** 41
[3] Vlček J 1989 A collisional–radiative model applicable to argon discharges over a wide range of conditions: I. Formulation and basic data *J. Phys. D: Appl. Phys.* **22** 623–31
[4] Bogaerts A, Gijbels R and Vlček J 1998 Collisional–radiative model for an argon glow discharge *J. Appl. Phys.* **84** 121
[5] Kano K, Suzuki M and Akatsuka H 2000 Spectroscopic measurements of electron temperature and density in argon plasmas based on collisional–radiative model *Plasma Sources Sci. Technol.* **9** 314–22
[6] Smith D J, Whitehead C J and Stewart R 2002 Complementary optical diagnostics for determination of rate coefficients and electron temperature in noble gas discharges *Plasma Sources Sci. Technol.* **11** 115–26
[7] Bezanahary T, Zissis G and Salo S A S 2003 A collisional radiative model applied to the study of pure rare gas electrical discharge *IEEE Trans. Plasma Sci.* **31** 587–95
[8] Dormand J R and Prince P J 1980 A family of embedded Runge–Kutta formulae *J. Comput. Appl. Math.* **6** 19–26
[9] Van Dyck R S Jr, Johnson C E and Shugart H A 1972 Lifetime lower limits for the $3P_0$ and $3P_2$ metastable states of neon, argon, and krypton *Phys. Rev.* A **5** 991–3
[10] Martin W C *et al* 2004 NIST Atomic Spectra Database http://physics.nist.gov/asd.
[11] Puech V and Mizzi S 1991 Collision cross sections and transport parameters in neon and xenon *J. Phys. D: Appl. Phys.* **24** 1974–85
[12] Tsurubuchi S, Arakawa K, Kinokuni S and Motohashi K 2000 Electron-impact cross sections of Ne *J. Phys. B: At. Mol. Opt. Phys.* **33** 3713–23
[13] Tsurubuchi S 2003 Electron-impact cross sections of Ne, private communication
[14] Chilton J E, Stewart M D Jr and Lin C C 2000 Electron-impact excitation cross sections of neon *Phys. Rev.* A **61** 052708-1
[15] Stewart M D Jr, Chilton J E, Boffard J B and Lin C C 2002 Use of radiation trapping for measuring electron-impact excitation cross sections for higher resonance levels of rare-gas atoms *Phys. Rev.* A **65** 032704-1
[16] Boffard J B, Keeler M L, Piech G A, Anderson L W and Lin C C 2001 Measurement of electron-impact excitation

cross sections out of the neon $^3P_2$ metastable level *Phys. Rev.* A **64** 032708
[17] Leveau J, Valignat S and Deigat F 1977 Destruction par chocs électroniques des atomes métastables et pseudo-métastables de néon dans une colonne positive *J. Physique Lett.* **38** L385
[18] Hyman H A 1981 Electron impact excitation cross sections for the transition $(n-1)p^5\,ns \rightarrow (n-1)p^5\,np$ in the rare gases *Phys. Rev.* A **24** 1094–5
[19] Boffard J B 2005 Electron-impact excitation cross sections out of the neon $1s_3$ and $1s_5$ level Private communication
[20] Rapp D and Englander-Golden P 1965 Total cross sections for ionization and attachment in gases by electron impact: I. Positive ionization *J. Chem. Phys.* **43** 1464–79
[21] Wetzel R C, Baiocchi F A, Hayes T R and Freund R S 1987 Absolute cross sections for electron-impact ionization of the rare-gas atoms by the fast-neutral-beam method *Phys. Rev.* A **35** 559–77
[22] Johnston M, Fujii K, Nickel J and Trajmar S 1996 Ionization of metastable neon by electron impact *J. Phys. B: At. Mol. Opt. Phys.* **29** 531–43
[23] Seaton M J 1998 Oscillator strength in Ne I *J. Phys. B: At. Mol. Opt. Phys.* **31** 5315–36
[24] Bogaerts A and Gijbels R 1997 Comparison of argon and neon as discharge gases in a direct-current glow discharge: a mathematical simulation *Spectrochim. Acta B* **52** 553–65
[25] Phelps A V 1959 Diffusion, de-excitation and three-body collision coefficients for excited neon atoms *Phys. Rev.* **114** 1011–25
[26] Leichner P K 1973 Time and pressure dependence of the vacuum-ultraviolet radiation in neon *Phys. Rev.* A **8** 815–22
[27] Ricard A 1996 *Reactive Plasmas* (Paris: SFV)
[28] Holstein T 1947 Imprisonment of resonance radiation in gases *Phys. Rev.* **72** 1212–33
[29] Molisch A F, Oehry B P, Schupita W and Magerl G 1993 Radiation-trapping in cylindrical and spherical geometries *J. Quant. Spectrosc. Radiat. Transfer* **49** 361–70
[30] Boffard J B, Lin C C and DeJoseph C A Jr 2004 Application of excitation cross sections to optical plasma diagnostics *J. Phys. D: Appl. Phys.* **37** R143–61
[31] Reader J, Sansonetti C J and Bridges J M 1996 Irradiances of spectral lines in mercury pencil lamps *Appl. Opt.* **35** 78–83
[32] Hagelaar G J M and Pitchford L C 2005 Solving the Boltzmann equation to obtain electron transport coefficients and rate coefficients for fluid models *Plasma Sources Sci. Technol.* **14** 722–33
[33] Capriati G, Colonna G, Gorse C and Capitelli M 1992 A parametric study of electron distribution functions and rate and transport coefficients in nonequilibrium helium plasmas *Plasma Chem. Plasma Process.* **12** 237–60
[34] Pack J L and Phelps A V 1961 Drift velocities of slow electrons in helium, neon, argon, hydrogen and nitrogen *Phys. Rev.* **121** 798–806
[35] Robertson A G 1972 The momentum transfer cross section for low energy electrons in neon *J. Phys. B: At. Mol. Phys.* **5** 648–64
[36] Kücükarpaci H N, Saelee H T and Lucas J 1981 Electron swarm parameters in helium and neon *J. Phys. D: Appl. Phys.* **14** 9–25
[37] Chanin L M and Rork G D 1963 Measurements of the first Townsend ionization coefficient in neon and hydrogen *Phys. Rev.* **132** 2547–53
[38] Kruithof A A and Penning F M 1937 *Physica* **4** 430